matched the refractive index of glass. Otto Schott formulated glass lenses that color-corrected objectives and produced the first *apochromatic* objectives in 1886. Köhler's crucial development of what has been termed *Köhler illumination* (discussed later) just after the turn of the century had a significant impact on microscopy and was possibly one of the most significant factors prior to the electronic age. Modern microscopes are all *compound* rather than *simple* microscopes since the image is magnified in two separate lens systems—the ocular and the objective. The following discussion covers both optical and electron microscopy; a comparison of both systems appears in Fig. 1.

Components of Microscopes

Nomenclature of Objectives. Several types of objectives, generally referred to as apochromatic, achromatic, and fluorite, are available for general microscopy. Achromatic objectives were first developed in the early nineteenth century by Lister and Amici, whose goal was to remove as much spherical and axial chromatic aberration as possible. Chromatic aberration prevents adequate imaging because the image if uncorrected will contain color fringes around fine structures. Correction is achieved by combining a convex lens of crown glass with a concave lens of flint glass. Fluorite objectives are made especially for fluorescence. Objectives are generally designed to be used with a cover glass having a thickness of 160 μm to 190 μm. Listed on each objective will be the key characteristics, as shown in Fig. 2.

Dry Objectives. High-quality objectives designed for use in air will usually have a correction collar. If the thickness of the cover glass differs from the ideal 170 μm, the correction collar must be adjusted to reduce spherical aberration.

Oil Immersion and Water Immersion. With objectives of high numerical aperture (NA) and high magnification, oil immersion will generally be necessary, as the resolution of a specimen is directly proportional to the NA. An objective designed for use with oil will always be clearly marked "oil". Specific oils of refractive index necessary to match the specimen and mounting conditions are desirable. For example, glass has an effective refractive index of 1.51 and oil must match this. The variation of refractive index with temperature must also be taken into account. It may be desirable to image an aqueous specimen through water. Water immersion objectives are available that can be placed directly into the suspending medium (which has an effective refractive index of approximately 1.33).

Light Sources. Most light sources for microscopy are arc lamps such as xenon, mercury, carbon, or zirconium arc lamps. These lamps generally have a life span of around 250 h, but recently lamps with life spans of 1000 h to 2000 h have been developed. The advantage of these light sources is the broad-spectrum excitation offered, stretching from 325 nm up to 700 nm. The excitation spectra of a mercury lamp and a mercury xenon lamp are compared in Fig. 3. It is possible to excite several fluorochromes simultaneously with these relatively inexpensive light sources.

MICROSCOPE IMAGE PROCESSING AND ANALYSIS

MICROSCOPY

History of Microscope Development

Prior to 1800 production microscopes using simple lens systems were of higher resolution than compound microscopes despite the achromatic and spherical aberrations present in the double convex lens design used. In 1812 W. H. Wollaston made a significant improvement to the simple lens, which was followed by further improvements over the next few years. Brewster improved upon this design in 1820. In 1827 Giovanni Battista Amici built high-quality microscopes and introduced the first matched achromatic microscope. He recognized the importance of cover-glass thickness and developed the concept of *water immersion.* Carl Zeiss and Ernst Abbe advanced oil immersion systems by developing oils that

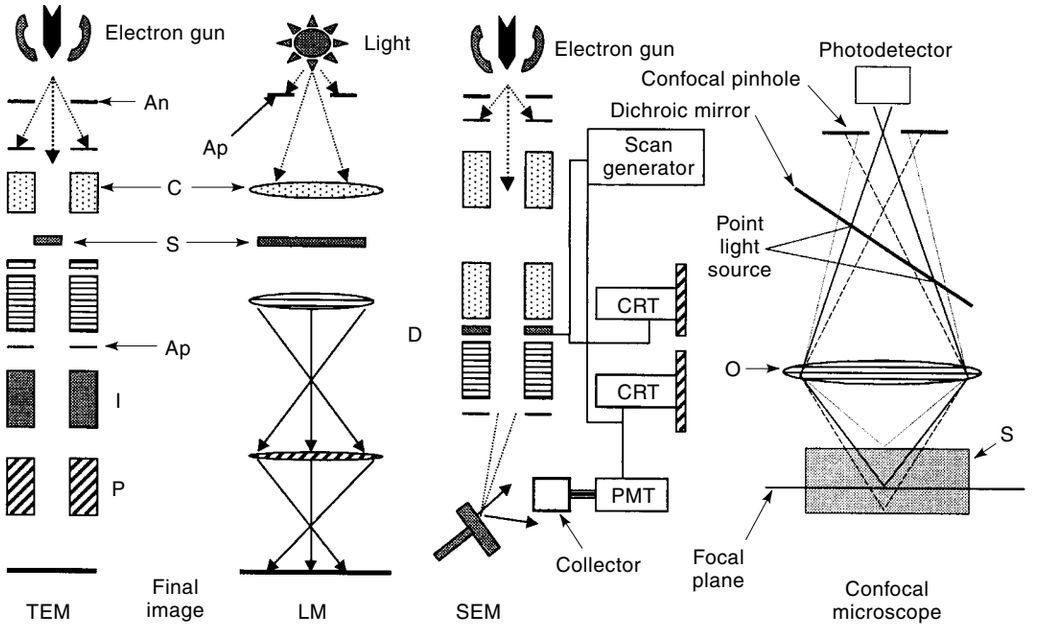

Figure 1. Comparison of image formation in electron and light microscopes.

Types of Optical Microscopes

160 mm Tube Length Microscope. Most commercial microscopes have been designed according to the International Standards Organization (ISO) standard, which was created to ensure that components (mainly objectives) were interchangeable. The standard, described in Fig. 4, specifies several key dimensions such as the length of the tube (160 mm), the parfocal distance of the objective (45 mm), and the object-to-image distance (195 mm).

Infinity-Corrected Microscopes. Recently many microscope manufacturers have switched to infinity-corrected optical systems. In this method of imaging, the traditional Telan optics (which are usually placed within 160 mm microscopes to allow insertion of other optical components) are replaced by a tube lens that forms a real, intermediate image and in which aberrations can be corrected. The placement of this tube lens allows the insertion of many optical components within the system because of its infinite image distance, its most significant advantage over the 160 mm systems.

Microscope Variations

Köhler Illumination. One of the most significant improvements in microscopy occurred at the beginning of the twentieth century when August Köhler developed the method of illumination still called *Köhler illumination.* Köhler also recognized that using shorter-wavelength light (UV) could improve resolution. The principle of Köhler illumination is that parallel light rays provide an evenly illuminated field of view while simultaneously the specimen is illuminated with a very wide cone of light. In Köhler illumination there are two conjugate planes formed with either image-forming planes or illuminating planes, which image the light source (filament). In order to observe the illuminating planes, it is necessary to focus on the objective back focal plane using a special telescope that replaces a regular ocular. Naturally the image planes are focused onto the specimen using the conventional ocular. The Köhler principle is shown in Fig. 5. While the efficiency of this system is not very high, it forms a very even illumination (the *bright field*), which is usually more important for quantitative purposes.

Phase Contrast. The development of phase-contrast microscopy resulted in a Nobel Prize for its inventor, Zernike, in

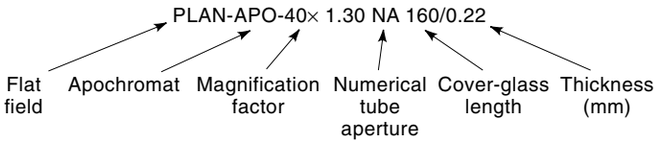

Figure 2. Objectives.

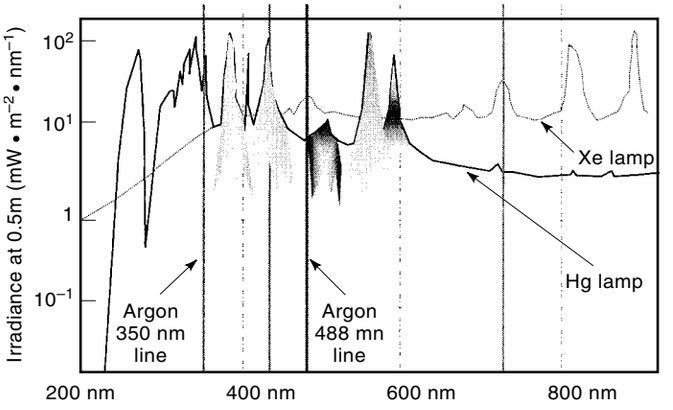

Figure 3. Arc lamp excitation spectra.

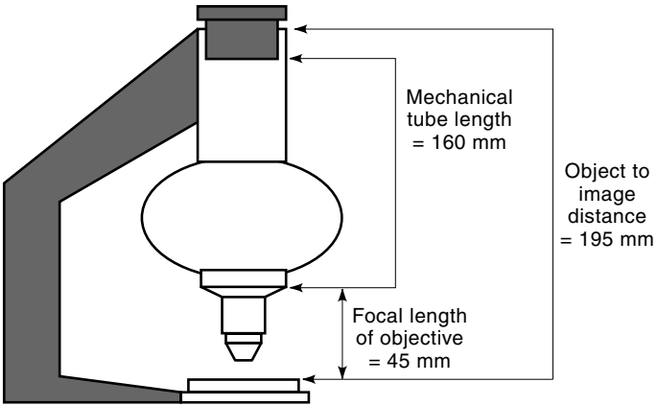

Figure 4. The conventional microscope.

1932. Phase contrast is essential to see details in specimens that have almost the same refractive index as the suspending or mounting medium. Changing the phase of the central beam by one quarter of a wavelength at the rear focal plane of the objective achieves fine detail and contrast. Essentially, an object that was previously transparent will now become absorbent, resulting in edges and organelles appearing dark with a light background.

Dark-Field Microscopy. In dark-field illumination, light is prevented from traveling through the objective because its angle is increased beyond the collection angle (the numerical aperture) of that objective. Thus, only highly diffracted light from granular or diffractive components or objects reaches the objective. Very small objects will be bright on a dark background.

Differential Interference Contrast (Nomarski Optics). Differential interference contrast microscopy requires the insertion of several additional components into the light path. Light travels through a polarizer through two critical components known as Wollaston prisms, which split the light into two parallel beams polarized at 45° with respect to each other. This light illuminates the specimen, which now by its nature creates an optical path difference. The light then passes through a second Wollaston prism, which essentially combines both beams, followed by an analyzer, which is oriented at 45° with respect to the vibration plane of either of the combined waves (giving equal intensity). Rotation of a polarizer increases or decreases one or the other component of the light. The shear created at the edge of the specimen will cause a halo, resulting in poor edge resolution if the Wollaston prisms are not matched to the resolution of the objective, necessitating customized prisms for every objective. For microscopy using epi-illumination, rather than transmitted light, a single Wollaston prism can be used.

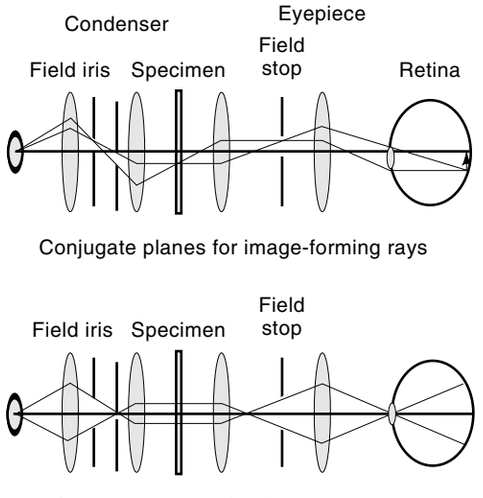

Figure 5. Köhler illumination.

Interference Reflection Microscopy. The principle of interference reflection depends upon passing the light through surfaces of different refractive index, resulting in constructive and destructive interference. When light is refracted in its immersion medium, a $\frac{1}{2}$ phase shift occurs, which when added to the resultant beam through each component (e.g., glass and medium) will cancel each other out as destructive interference. The further the specimen is from the coverslip the brighter the reflectance will be, and the closer, the darker the reflectance, such that at the contact point of the coverslip and the medium no effective illumination will be observed.

Fluorescence Microscopy. In fluorescence microscopy light of one wavelength excites fluorescent molecules within or attached to the specimen, and the emitted light of a longer wavelength is collected. This means that only molecules that are fluorescent will be imaged in such a system. Most fluorescent microscopes use mercury arc lamps as excitation sources, with selection of specific excitation wavelength being made by excitation filters and dichroic beam splitters to separate the excitation light from the emitted signal.

ELECTRON MICROSCOPY

Principles

1. Comparison of image formation in electron and light microscopes
2. Preparation of biological samples
3. Digital imaging in electron microscopes
4. Image acquisition and storage
5. Image processing
6. Model-based and design-based image analysis

Figure 1 is a schematic comparison of a transmission electron microscope (TEM), a light microscope (LM), and a scanning electron microscope (SEM). The TEM and SEM use a beam of electrons as the illumination source, as opposed to photons for the LM. The geometric optics of image formation in the TEM is identical to the LM. The only difference is that focusing is accomplished with electromagnetic lenses in the TEM and glass lenses in the LM. In the TEM and SEM, illumination is most commonly generated by thermally emitted electrons from a tungsten filament. The amount of illumination from an electron gun or the *brightness* (β) is defined as $\beta = \rho_e eV/kT$, where ρ_e is the cathode current density, e the elec-

tronic charge, V the accelerating voltage, k Boltzmann's constant, and T the absolute temperature. The brightness β is proportional to V; therefore increasing the accelerating voltage will increase the illumination. The electron gun, the condenser lens (C) system, and the anode (An) form the illuminating system of the microscope. The electron gun consists of the filament or cathode and an electron-gun cap. The electron gun is self-biased, and the bias voltage applied to the gun cap controls the area of electron emission in the filament. Any increase in the beam current causes an increase in the bias voltage, which acts to reduce the beam current again. Below the gun cap is an anode that is held at ground potential. The electrons are accelerated by the potential difference between the cathode and the anode. Apertures (Ap) in each of the microscopes control illumination. In the TEM and LM the illumination is transmitted through the specimen (S) and focused by an objective lens (O), which is the source of the resolving power. After passing through the objective lens the image is further magnified by intermediate (I) and projector lenses (P) in the TEM and by the lens in the eyepiece in the LM. The final image for the TEM is projected onto a fluorescent screen and for the LM onto the retina of the eye. The illumination system of the SEM is the same as that of the TEM, but deflection coils (D) are used to raster the electron beam across the specimen. As the electron beam scans the specimen it generates a variety of secondary electromagnetic radiation that may be analyzed. Low-energy secondary electrons (<50 eV) that escape from the surface of the specimen contain the surface detail information. These electrons impinge upon a scintillator located at one end of a quartz light pipe, where they are collected and converted into light pulses that are conducted via this light pipe to a photomultiplier tube (PMT) for amplification. The signal is then processed so that it can be displayed on cathode ray tubes (CRTs).

Preparation Methods

In order to understand image processing and analysis of electron microscopic images it is important to have some appreciation of the preparation methods and sample sizes for the specimens that are the subject of the analysis. Biological specimens for transmission or scanning electron microscopy need to have their "normal" structure stabilized via chemical or physical preservation (fixation). The usual chemical fixative is a buffered solution of 2% to 3% glutaraldehyde. This five-carbon aldehyde has two reactive groups that cross-link proteins by forming methylene bridges between polypeptides at reactive side groups, especially active amino and imino groups. The solution is usually slightly hypertonic (400 mOsm to 500 mOsm).

Glutaraldehyde

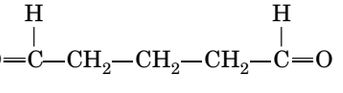

The glutaraldehyde preserves primarily the protein components of tissues but does not preserve lipid components, which require a secondary fixative such as osmium tetroxide (OsO_4).

After rapid removal from the body, tissues may be fixed by immersion and then minced into 1 mm^3 pieces while still submerged in fixative. The rate of fixation may be increased via microwave irradiation procedures. Alternatively, an anesthetized animal may have the blood replaced by the fixative by either whole body perfusion or cannulation and perfusion of a specific organ.

After fixation, specimens are dehydrated through a solvent gradient (i.e., 30%, 60%, 90%, 100%), generally acetone or alcohol. This allows the infiltration of the tissue with an embedding resin (most commonly epoxy and acrylic resins) that will be cured and hardened. The embedding resin acts as a support for the tissue, which will be thin-sectioned (50 nm to 90 nm) for examination in the TEM. The images obtained from a thin section perhaps 0.5 mm^2 in area will be the subject of the image analysis. With the current computational power and relative ease of extracting data from images, it is simple to generate large amounts of meaningless data. Therefore, the sampling procedures to be used in collecting data are critical for the measurements to be valid. Unbiased sampling procedures are the basis for modern morphological and stereological image analysis. Anyone embarking upon computerized analysis should refer to the stereology literature on sampling before beginning an experiment. The areas for image analysis are best sampled in a systematic manner independent of the content during both the collection and photographic process.

Digital Imaging in the Electron Microscope

In order to perform image processing and analysis, images must be converted into a digital form. In the 1990s, digital image acquisition has become the standard for scanning electron microscopes. Since the image in the SEM starts as an electronic signal, it is relatively easy to convert and display the image in digital format. Until recently, the resolution capabilities of digital acquisition devices were not suitable or were cost prohibitive for direct digital acquisition in transmission electron microscopes. However, the technology has progressed very rapidly and as the cost of high-resolution charge-coupled device (CCD) cameras drops, digital image acquisition is expected to be the rule and not the exception for most commercial TEM microscopes by the end of the century.

Image Acquisition

Since current SEMs are all digital, this discussion will focus on TEMs. For microscopes that utilize the traditional film format, the negative may be digitized using flat-bed scanners that have a transparency adapter. Scanning resolutions of 600 dpi or greater are common on today's equipment and are suitable for all but the most demanding analysis, which may require high-resolution drum scanners. It is important that analysis be performed on nonpixelated images. If individual pixels are evident, then the analysis will not be accurate. The pixel depth is also important for analysis of the image. While all flat-bed scanners will provide 8-bit gray-scale resolution, flat-bed scanners that have the capability to capture10-bit gray-scale or higher can take advantage of the contrast resolution present in an electron microscopic negative. When processing the image the greater pixel depth may be utilized to enhance features of interest.

A variety of CCD cameras is currently available for direct image acquisition in the TEM. Cameras with a video rate of acquisition are useful for demonstrating images to groups of individuals and may be useful for basic image analysis such as cell counting. Slow-scan digital cameras such as the Gatan Megascan (2048 × 2048 pixels) and Kodak Megaplus (4096 ×

4096 pixels) are capable of producing high-quality digital images in the electron microscope. One advantage of CCD cameras is that they can perform binning operations. The output from an array of pixels (e.g., 6 × 6 pixels) may be combined into one pixel. Although this reduces resolution, it also increases sensitivity and allows the rapid collection of information from electron-beam-sensitive specimens using minimal illumination. If the objects of interest are present, then a final high-resolution image that does not utilize binning may be captured.

CONFOCAL MICROSCOPY

Principles

The original patent for the confocal microscope was filed by Marvin Minsky at Harvard University in 1957. Successive developments were made by Brackenhoff, Wijnaendts van Resandt, Carlesson, Amos, and White, among others. A confocal microscope achieves crisp images of structures even within thick tissue specimens by a process known as optical sectioning. The source of the image is photon emission from fluorescent molecules within or attached to structures within the object being sectioned. A point source of laser light illuminates the back focal plane of the microscope objective and is subsequently focused to a diffraction-limited spot within the specimen. At this point the fluorescent molecules are excited and emit light in all directions. However, because the emitted light refocuses in the objective image plane (being conjugate with the specimen), and because the light passes through a pinhole aperture that blocks out-of-focus light, an image of only a thin optical section of the specimen is formed. Out-of-focus light is effectively removed from the emission, creating a "clean" image, as opposed to the traditional fluorescent microscope that includes all this out-of-focus light (Fig. 6a). It is possible to increase the "depth" of the optical section by varying the diameter of the pinhole, which effectively increases the light collection from the specimen. However, this also decreases the resolution. The resolution of a point light source in this image plane is a circular Airy diffraction pattern with a central bright region and outer dark ring. The radius of this central bright region is defined as $r_{\text{Airy}} = 0.61\lambda/\text{NA}$, where r_{Airy} is a distance in the specimen plane, λ is the wavelength of the excitation source, and NA is the numerical aperture of the objective lens. To increase the signal and decrease the background light, it is necessary to decrease the pinhole to a size slightly less than r_{Airy}; a correct adjustment can decrease the background light by a factor of 10^3 over conventional fluorescence microscopy. Therefore pinhole diameter is crucial for achieving maximum resolution in a thick specimen. This becomes a tradeoff, however, between increasing axial resolution (optimum = $0.7r_{\text{Airy}}$) and lateral resolution (optimum = $0.3r_{\text{Airy}}$).

There are several methods for achieving a confocal image. One common method is to scan the point source over the image using a pair of galvanometer mirrors, one of which scans in the X and the other in the Y direction. The emitted fluorescence emission traverses the reverse pathway and is collected instantaneously. It is separated from the excitation source by a beam-splitting dichroic mirror that reflects the emission to a photomultiplier tube that amplifies the signal, passes it to an analog-to-digital converter (ADC), and displays

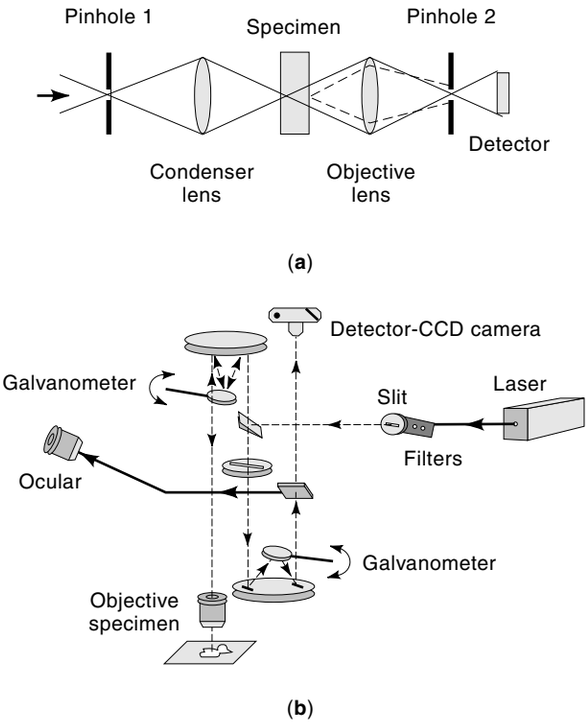

Figure 6. (a) How a confocal image is formed. Modified from J. B. Pawley, Handbook of Biological Confocal Microscopy, New York: Plenum Press, 1989. (b) Principles of a line scanner.

the signal as a sequential raster scan of the image. Most current systems utilize 16-bit ADCs, allowing an effective image of 1024 × 1024 pixels or more with at least 256 gray levels. Some confocal microscopes can collect high-speed images at video rates (30 frames/s), while others achieve faster scanning by slit-scanning (see below).

Recently, two-photon excitation has been demonstrated in which a fluorophore simultaneously absorbs two photons, each having half the energy normally required to raise the molecule to its excited state. A significant advantage of this system is that only the fluorophore molecules in the plane of excitation can be excited, as this is the only area where the light intensity is sufficient. Therefore even less background noise is collected and the efficiency of imaging thick specimens is significantly increased. Two-photon excitation has an added advantage for those probes requiring UV excitation (see later), which has a tendency to damage tissue (particularly when imaging live cells); the two-photon system can achieve UV excitation without damage to the tissue.

Benefits of Confocal Microscopy. Confocal microscopy has become a familiar tool in the research laboratory with a number of significant advantages over conventional fluorescence microscopy. Among these are the following:

Reduced blurring of the image from light scattering. As explained previously, since out-of-focus light is excluded from the image plane, it is possible to collect sharper images than with regular fluorescent microscopes. Photons emitted from points outside the image plane are rejected.

Increased effective resolution. This occurs by virtue of the increased resolution observed from a point source of light imaged through a pinhole.

Improved signal-to-noise ratio. Decreased background light allows significantly improved signal-to-noise ratio.

Z-axis scanning. A series of optical sections can be obtained at regular distances by moving the objective progressively through the specimen in the vertical direction.

Depth perception in Z-sectioned images. With software reconstruction techniques, it is possible to reconstruct an image of the fluorescence emission of the specimen through the entire depth of the specimen.

Electronic magnification adjustment. By reducing the scanned area of the excitation source, but retaining the effective resolution, it is possible to magnify the image electronically.

Light Sources

The most common light sources for confocal microscopes are lasers. The acronym LASER stands for light amplification by stimulated emission of radiation; the nature of laser operation is detailed elsewhere. Most lasers on conventional confocal microscopes are continuous wave (CW) lasers and are gas lasers, dye lasers, or solid-state lasers. The most popular gas laser is argon-ion (Ar), followed by either krypton-ion (Kr) or a mixture of argon and krypton (Kr-Ar). Helium-neon (He-Ne) and helium-cadmium (He-Cd) are also used in confocal microscopy. The He-Cd provides UV lines at 325 nm or 441 nm, while the argon-ion lasers can emit 350 nm to 363 nm UV light if the laser is powerful enough. Otherwise the most common wavelength for fluorescent molecule excitation is 488 nm [ideal for fluorescein-isothiocyanate (FITC)] and either 543 nm (green He-Ne), 568 nm, or 647 nm (Kr-Ar).

The power necessary to excite fluorescent molecules at a specific wavelength can be calculated. For instance, consider 1 mW of power at 488 nm focused via a 1.25 NA objective to a Gaussian spot whose radius at $1/e^2$ intensity is 0.25 μm. The peak intensity at the center will be 10^{-3} W $\pi(0.25 \times 10^{-4}$ cm$)^2 = 5.1 \times 10^5$ W/cm^2 or 1.25×10^{24} photons/(cm$^2 \cdot$s^{-1}). At this power, FITC would have 63% of its molecules in an excited state and 37% in ground state at any one time.

The great majority of confocal microscopes are designed around conventional microscopes, but as discussed above, the light source can be one of several lasers. For most cell biology studies, arc lamps are not adequate sources of illumination for confocal microscopy. When using multiple laser beams, it is vital to expand the laser beam using a beam-expander telescope so that the back focal aperture of the objective is always completely filled. If several different lasers are used, the beam widths must also be matched if simultaneous excitation is required. The most important feature in selecting the laser line is the absorption maximum of the fluorescent probe. Examples of almost ideal excitation of probes can be seen in Table 1, which shows the maximum excitation in percent of several probes excited by the three primary lines available from a Kr–Ar laser—a common excitation source for confocal microscopes.

Line Scanners

The principal reason for using a line scanner is to obtain rapid successive images of a fluorescence emission. One of the limiting factors that must be addressed in confocal microscopy is photobleaching of the fluorophor with intense illumination. By scanning a *line* of laser light across the specimen instead of a point of light, even illumination of lower intensity can be applied to the specimen at high rates. In general, these instruments are referred to as *slit-scanners* because they utilize a slit aperture, which can either scan or remain stationary. The detector for these scanners is usually a sensitive video camera—SIT, ISIT, or cooled CCDs. An example of the light path of one such slit-scanner is shown in Fig. 6b.

Table 1. Excitation and Emission Peaks

Fluorophore	Excitation Peak (nm)	Emission Peak (nm)	% Max Excitation at 488 nm	% Max Excitation at 568 nm	% Max Excitation at 647 nm
FITC	496	518	87	0	0
Bodipy	503	511	58	1	1
Tetra-M-Rho	554	576	10	61	0
L-Rhodamine	572	590	5	92	0
Texas Red	592	610	3	45	1
CY5	649	666	1	11	98

Note: You will not be able to see CY5 fluorescence under the regular fluorescent microscope because the wavelength is too high.

Fluorescent Probes

Many fluorescent probes are available for use in confocal microscopy: probes for protein (Table 2), probes for organelles (Table 3), probes for nucleic acids (Table 4), probes for ions (Table 5), probes for pH indicators (Table 6), and probes for oxidation states (Table 7). The excitation properties of each probe depend upon its chemical composition. Ideal fluorescent probes will have a high quantum yield, a large Stokes shift, and nonreactivity with the molecules to which they are bound. It is vital to match the absorption maximum of each probe to the appropriate laser excitation line. For fluorochrome combinations, it is desirable to have fluorochromes with similar absorption peaks but significantly different emission peaks, enabling use of a single excitation source. It is common in confocal microscopy to use two, three, or even four distinct fluorescent molecules simultaneously.

Photobleaching

Photobleaching is defined as the irreversible destruction of an excited fluorophore by light. Uneven bleaching through a

Table 2. Probes for Proteins

Probe	Excitation (nm)	Emission (nm)
FITC	488	525
PE	488	525
APC	630	650
PerCP™	488	680
Cascade Blue	360	450
Coumarin-phalloidin	350	450
Texas Red™	610	630
Tetramethylrhodamine-amines	550	575
CY3 (indotrimethinecyanines)	540	575
CY5 (indopentamethinecyanines)	640	670

Table 3. Specific Organelle Probes

Probe	Site	Excitation (nm)	Emission (nm)
BODIPY[a]	Golgi	505	511
NBD[b]	Golgi	488	525
DPH[c]	Lipid	350	420
TMA[d]-DPH	Lipid	350	420
Rhodamine 123	Mitochondria	488	525
DiO[e]	Lipid	488	500
DiI-C_n-(5)[f]	Lipid	550	565
DiO-C_n-(3)[g]	Lipid	488	500

[a] BODIPY: borate-dipyrromethene complex.
[b] NBD: nitrobenzoxadiazole.
[c] DPH: diphenylhexatriene.
[d] TMA: trimethylammonium.
[e] DiO: DiO-C_{18}-(3)-3,3′-dioctadecyloxacarbocyanine perchlorate.
[f] DiI-C_n-(5): 1,1′-di“n”yl-3,3,3′,3′-tetramethylindocarbocyanine perchlorate.
[g] DiO-C_n-(3): 3,3′-di“n”yl oxacarbocyanine iodide.

specimen will bias the detection of fluorescence, causing a significant problem in confocal microscopy. Methods for countering photobleaching include shorter scan times, high magnification, high NA objectives, and wide emission filters as well as reduced excitation intensity. A number of *antifade* reagents are available; unfortunately, many are not compatible with viable cells.

Antifade Reagents. Many quenchers act by reducing oxygen concentration to prevent formation of excited species of oxygen, particularly singlet oxygen. Antioxidants such as propyl gallate, hydroquinone, and *p*-phenylenediamine, while fine for fixed specimens, are not satisfactory for live cells. Quenching fluorescence in live cells is possible using systems with reduced O_2 concentration or using singlet-oxygen quenchers such as carotenoids (50 mM crocetin or etretinate in cell cultures), ascorbate, imidazole, histidine, cysteamine, reduced glutathione, uric acid, and trolox (vitamin E analog). Photobleaching can be calculated for a particular fluorochrome such as FITC—at 4.4×10^{23} photons $\cdot$ cm$^{-2} \cdot$ s^{-1} FITC bleaches with a quantum efficiency Q_b of 3×10^{-5}. Therefore FITC would be bleaching with a rate constant of 4.2×10^3 s^{-1}, so 37% of the molecules would remain after 240 μs of irradiation. In a single plane, 16 scans would cause 6% to 50% bleaching.

Applications

Neuroscience. Evaluation of neuronal tissue is a classic application of confocal microscopy. One example is the identification and tracking of nerve cells. Typically neurons are injected with a fluorescent dye such as Lucifer yellow; three-dimensional projections are made to identify the structure and pathway of the neuron.

Table 4. Probes for Nucleic Acids

Hoechst 33342 (AT[a] rich) (UV)
DAPI[b] (UV)
PI[c] (UV or visible)
Acridine Orange (visible)
TOTO-1, YOYO-3, BOBO[d] (visible)
Pyrine Y (visible)
Thiazole Orange (visible)

[a] AT: Adenine/Thymine.
[b] DAPI: 4′,6-diamidino-2-phenylindole.
[c] PI: propidium iodide.
[d] TOTO, YOYO, BOBO: dimeric cyanine dyes for nucleic acid staining molecular probes proprietary.

Table 5. Probes for Ions

Probe	Excitation (nm)	Emission (nm)
INDO-1	350	405, 480[a]
QUIN-2	350	490
Fluo-3	488	525
Fura-2	330, 360	510

[a] Optimal—it may be more practical to measure at 400, 525 nm.

Cell Biology. The applications in cell biology are too numerous to cover in this section. However, one of the most useful applications currently is cell tracking using green fluorescent protein (GFP), a naturally occurring protein in the jellyfish *Aequorea victoria,* which fluoresces when excited by UV or blue light. A fluorescent protein (GFP) can be transfected into cells so that subsequent replication of the organism carries with it the fluorescent reporter molecule, providing a valuable tool for tracking the presence of that protein in developing tissue or differentiated cells. This is particularly useful for identifying regulatory genes in developmental biology and for identifying the biological impact of alterations to normal growth and development processes. In almost any application, multiple fluorescent wavelengths can be detected simultaneously. For instance, the fluorescent dyes Hoechst 33342 (420 nm), FITC (525 nm), and Texas Red (630 nm) can be simultaneously collected to create a three-color image (or more if more detectors are available), providing excellent information regarding the location and relationships between the labeled molecules and the structures they identify.

Living Cells. Evaluation of live cells using confocal microscopy presents some difficult problems. One of these is the need to maintain a stable position while imaging a live cell. For example, a viable respiring cell, even when attached to a matrix of some kind, may be constantly changing shape, preventing a finely resolved three-dimensional (3-D) image reconstruction. Fluorescent probes must be found that are not toxic to the cell. Hoechst 33352 is a cell-permeant DNA probe that can be used to label live cells. Figure 7 presents an example in which there was a need to identify and enumerate cells attached to an extracellular matrix. In this image the cells can be accurately enumerated and their relative locations within the matrix determined as well. This figure demonstrates the effectiveness of confocal microscopy as a qualitative and quantitative tool for creating a 3-D image reconstruction of these live cells. The image is in three parts: (a) a 3-D

Table 6. pH Sensitive Indicators

Probe	Excitation (nm)	Emission (nm)
SNARF-1[a]	488	575
BCECF[b]	488	525, 620
	440, 488	525

[a] SNARF: seminaphthorhodafluor.
[b] BCECF: 2′,7′-bis-(carboxyethyl)-5,6-carboxyfluorescein.

Table 7. Probes for Oxidation States

Probe	Oxidant	Excitation (nm)	Emission (nm)
DCFH-DA[a]	H_2O_2	488	525
HE[b]	O_2^-	488	590
DHR 123[c]	H_2O_2	488	525

[a] DCFH-DA: dichlorofluorescin diacetate.
[b] HE: hydroethidine.
[c] DHR-123: dihydrorhodamine 123.

Figure 8. Example of 3-D reconstruction. Cells grown on a cover glass were imaged by confocal microscopy and then reconstructed as they had been on the original coverslip.

reconstruction of the material; (b) a pseudo-red/green image that requires red/green glasses to see the 3-D effect; and (c) a rotation of the image at 30° from the plane of collection. Figure 8 is another example of 3-D imaging of live cells, in this case endothelial cells growing on glass in a tissue culture dish. Thirty image sections were taken 0.2 μm apart; the image plane presented shows an X–Z plane with the cells attached to the cover glass. The cover glass is represented by a cartoon insertion to show where the cells would be actually attached.

Ratio Imaging. Confocal microscopy can be used for evaluation of physiological processes within cells. Examples are changes in cellular pH, changes in free Ca^{2+} ions, and changes in membrane potential and oxidative processes within cells. These studies require simultaneous fluorescence emission ratioing of the fluorescence molecules in real time. Usually these molecules are excited at one wavelength but emit at two wavelengths depending upon the change in properties of the molecule. For example, changes in cellular pH can be identified using BCECF (2′,7′-bis(carboxyethyl)-5(and 6)-carboxyfluorescein) which is excited at 488 nm and emits at 525 nm and 590 nm. The ratio of 590 nm to 525 nm signals reflects the intracellular pH. Similarly, INDO-1, a calcium indicator, can be excited at 350 nm to measure the amount of Ca^{2+} in a cell. The ratio of 400 nm to 525 nm emission signals reflects the concentration of Ca^{2+} in the cell; INDO-1 can bind Ca^{2+}, and the fluorescence of the bound molecule is preferentially at the lower emission wavelength. Rapid changes in Ca^{2+} can be detected by kinetic imaging—taking a series of images at both emission wavelengths in quick succession. An example is shown in Fig. 9.

Fluorescence Recovery after Photobleaching. Fluorescence recovery after photobleaching (FRAP) is a measure of the dynamics of the chemical changes of a fluorescent molecule within an object such as a cell. A small area of the cell is bleached by exposure to an intense laser beam, and the recovery of fluorescent species in the bleached area is measured. In such a case the recovery time (t) can be calculated from the equation $t = W^2/4D$, where W is the diameter of the bleached spot and D is the diffusion coefficient of the fluorescent molecule under study. An alternative technique can measure interactions between cells; one of two attached cells is bleached and the recovery of the pair as a whole is monitored. Figure 10 demonstrates such a setup.

Diagnostic Pathology. The use of confocal microscopy in diagnostic pathology is a developing field. The key advantages of the confocal system relate to the increased resolution, the ability to create 3-D views (stereoscopic images), and the more advanced image analysis that usually accompany these instruments. Some particular advantages are in evaluation of skin diseases and of cell growth in tissue injury and repair.

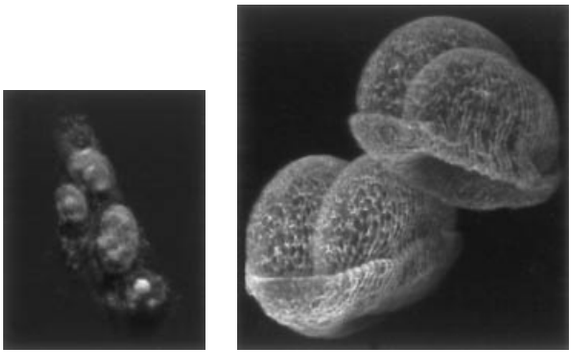

(**a**) (**b**)

Figure 7. (a) Projection of endothelial cells labeled with hydroethdine imaged at 488 nm excitation and 575 nm emission. Fluorescence measured is for ethidium bromide, the product of oxidation of the hydroethidine. (b) Reconstruction of pollen grains from a confocal image of 30 optical sections.

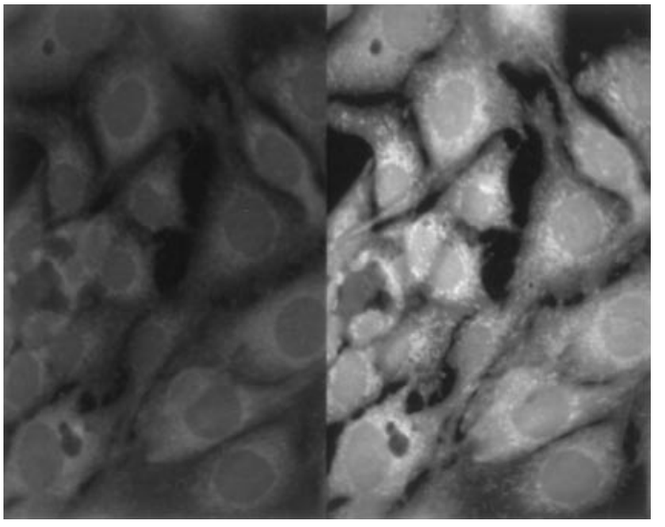

Figure 9. Calcium flux measurements. Pulmonary artery endothelial cells loaded with Indo-1, a fluorescent probe for calcium. The presence of calcium can be quantitated by measuring the ratio of fluorescence emission at two wavelengths—400 nm (left box) and 525 nm (right box).

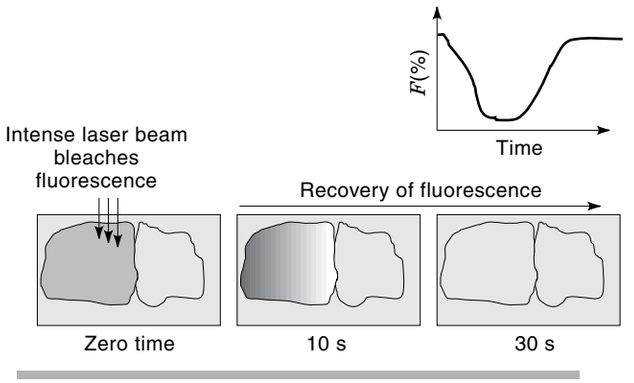

Figure 10. Fluorescence recovery after photobleaching.

IMAGE ANALYSIS

2-D Image Processing

Image processing is the procedure of feature enhancement prior to image analysis. Image processing is performed on *pixels* (smallest units of digital image data). The various algorithms used in image processing and morphological analysis perform their operations on groups of pixels (3×3, 5×5, etc.) called *kernels*. These image-processing kernels may also be used as structuring elements for various image morphological analysis operations.

The diagram

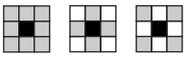

represents a series of 3 pixel $\times$ 3 pixel kernels (left to right A, B, C). Many image-processing procedures will perform operations on the central (black) pixel using information from neighboring pixels. In kernel A, information from all the neighbors is applied to the central pixel. In kernel B, only the strong neighbors, those pixels vertically or horizontally adjacent, are used. In kernel C, only the weak neighbors, those diagonally adjacent, are used in the processing. Various permutations of these kernel operations form the basis for digital image processing. At this point it is necessary to define some of the properties of digital images and the principles that guide mathematical morphology.

A Euclidean binary image may be considered as a subset of n-dimensional Euclidean space $\mathbb{R}^n$. A binary image may be represented by the set

$$X = \{z : f(z) = 1, z = (x, y) \in \mathbb{R}^2\}$$

The background of a binary object is the set X^c.

$$X^c = \{z : f(z) = 0, z = (x, y) \in \mathbb{R}^2\}$$

The function f is the characteristic function of X.

If the Euclidean grid $\mathbb{Z}^2$ is used instead of $\mathbb{R}^2$, then the definition for binary images becomes

$$X = \{(i, j) : f(i, j) = 1, z = (i, j) \in \mathbb{Z}^2\}$$
$$X^c = \{(i, j) : f(i, j) = 0, z = (i, j) \in \mathbb{Z}^2\}$$

Mathematical morphology may also be used to describe gray-scale (multivalue) objects. Gray-scale objects are functions of $f(x, y)$ of the two spatial coordinates $x, y, (x, y) \in \mathbb{R}^2$

$$(x, y) \in \mathbb{R}^2 \rightarrow f(x, y) \in \mathbb{R}$$

The gray-scale images may be viewed as subsets of the Cartesian product $\mathbb{R}^2 \times \mathbb{R}$. If the gray-scale image is of the form $f(i, j)$, $(i, j) \in \mathbb{Z}^2$, then it may be represented as a subset of $\mathbb{Z}^2 \times \mathbb{R}$.

Mathematical morphological operations utilize a structuring element (usually a round or square kernel) to probe an image. The interaction of the probe with the image is the morphological transformation $\psi(X)$. Measurements (m) derived from $\psi(X)$ need to meet several principles if the morphological transformation is to be quantitative. These principles form the foundation for model-based image analysis.

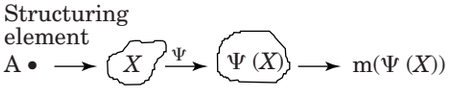

The first principle is *translation invariance*. This means that the structure of an object does not change with its position in space.

If X_z is the translate of the set $X \subset \mathbb{R}^2$ by some vector $z \in \mathbb{R}^2$ the translation invariance is stated

$$\psi(X_z) = [\psi(X)]_z$$

The second principle of mathematical morphology is *compatibility with change of scale*. A transformation of an object may not change the object's structure. A morphological transformation $\psi(X)$ is valid if, for some scaling factor λ, the following transformation $\psi_\lambda(X)$ is true:

$$\psi_\lambda = \lambda\psi(\lambda^{-1}X)$$

The third principle is *local knowledge*. Since objects are viewed through image frames or windows, it is necessary that any window M^* contain enough information (local knowledge as opposed to global knowledge) such that the transformation $\psi(X)$ may be performed.

$$[\psi X \cap M)] \cap M^* = \psi(X) \cap M^*$$

The fourth principle is *semicontinuity*. If A is included in B then $\psi(A)$ should be included in $\psi(B)$. If X_n is a sequence of closed objects tending toward the limit image of object X, and $\psi(X_n)$ is the sequence of the transformed objects, then the transformations are semicontinuous if the sequence of transformed objects tends to $\psi(X)$.

These four principles are fundamental to many of the image-processing and analysis functions. Two of the most basic mathematical morphological operations are erosion and dilation. These are based upon Minkowski set addition and subtraction.

If the image (A) is probed by the structuring element (B), the *erosion* of set A by set B is defined by $A \ominus B = \{x: B = x < A\}$.

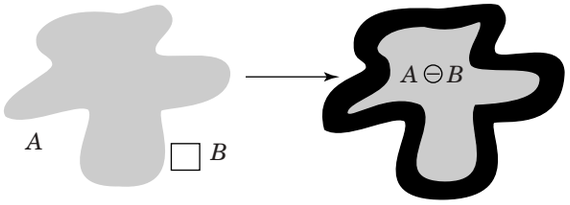

In mathematical morphology the complementary operation to erosion is *dilation*. The dilation of set A by structuring element B is defined by $A \oplus B = [A^c \ominus (-B)]^c$, where A^c is the set theoretic complement of A.

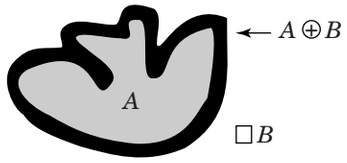

Image Enhancement

With the background just described on some of the principles of mathematical morphology we can now examine some basics of image processing and analysis. Simple image-processing techniques to change the brightness and contrast enhancement may be performed on look-up tables (LUT). Input look-up tables allow manipulation of the image data prior to saving the image in digital format. To utilize an input LUT, a frame grabber is needed. The output LUT displays the data after storage in digital format in a frame buffer or storage device. In an 8-bit gray-scale image, a level of zero (0) represents black and a level 255 represents white. In Fig. 11 the SEM image in the upper left is represented by the histogram (output LUT) in the lower left. The histogram shows that the image does not contain gray values at the upper or lower end. If the histogram is adjusted to make the levels more uniform as represented in the middle histogram, this stretches the range of gray values from 0 to 255. The resulting image and stretched histogram are represented in the upper and lower right frames. It is important to understand that the processed image on the right does not have greater resolution and is not inherently a better image than the one on the left. Because human vision is very sensitive to differences in contrast, the image on the right appears better but is not actually improved.

Filtering Methods—Noise Reduction. Images collected under low illumination conditions may have a poor signal-to-noise ratio. The noise in an image may be reduced using image-averaging techniques during the image acquisition phase. By using a frame grabber and capturing and averaging multiple frames (e.g., 16 to 32 frames), one can increase the information in the image and decrease the noise. Cooled CCD cameras have a better signal-to-noise ratio than noncooled CCD cameras. Utilizing spatial filters may also decrease noise in a digital image.

Filters such as *averaging* and *Gaussian* filters will reduce noise but also cause some blurring of the image, so their use on high-resolution images is usually not acceptable. *Median* filters cause minimal blurring of the image and may be acceptable for some electron microscopic images. These filters use a kernel such as a 3×3 or 5×5 to replace the central or target pixel luminance value with the median value of the neighboring pixels. Periodic noise in an image may be removed by editing a 2D fast Fourier transform (FFT). A forward FFT of the image in Fig. 12 allows one to view the periodic noise (center panel) in an image. This noise, as indicated

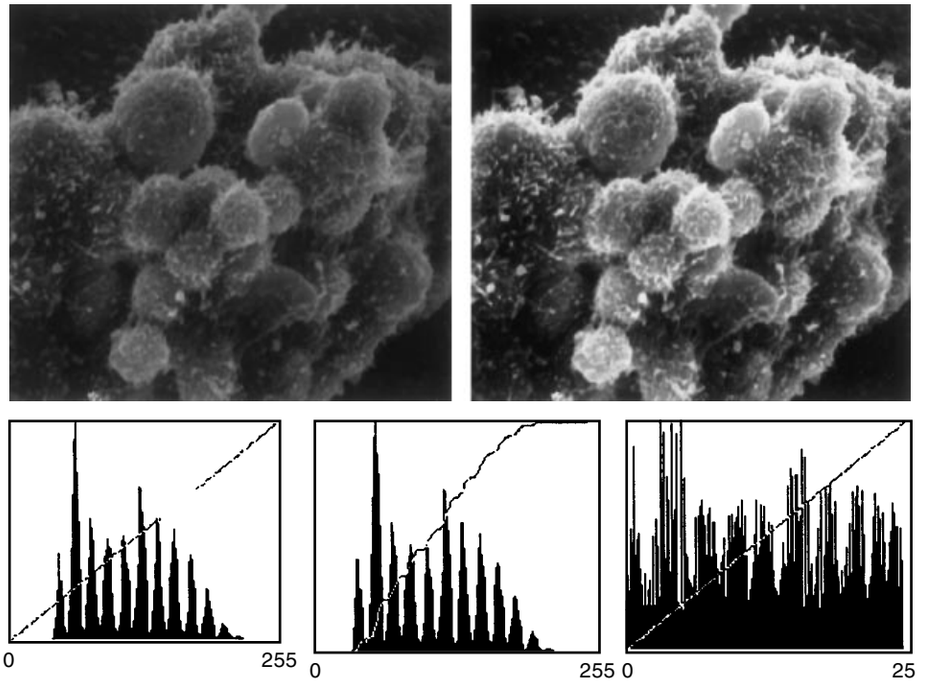

Figure 11. Scanning electron micrograph of cultured cells. The histograms represent gray-scale distribution. Left, original image, which does not cover the entire gray-scale range. Right, image obtained when gray-scale histogram is stretched to cover the entire range. See text for detailed explanation.

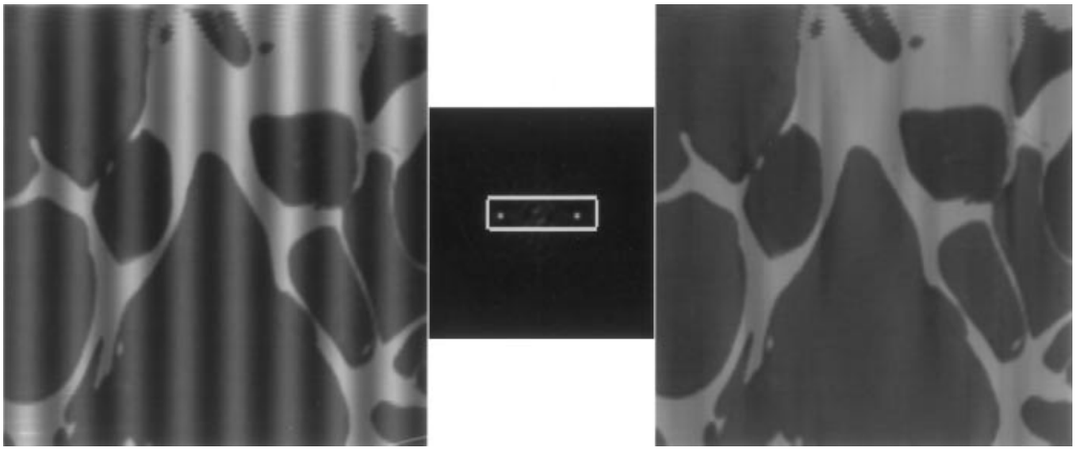

Figure 12. FFT analysis of image performed using Optimas.

by the white box, may be edited from the image and then an inverse Fourier transform performed to restore the image without the noise (right panel).

Image Analysis

After adjustment for contrast and brightness and for noise, the next phase of the process is feature identification and classification. Most image data may be classified into areas that feature closed boundaries (e.g., a cell), points (discrete solid points or objects that may be areas), and linear data. For objects to be identified they must be segmented and isolated from the background. It is often useful to convert a gray-scale image to binary format (all pixel values set to 0 or 1). Techniques such as image segmentation and edge detection are easily carried out on binary images but may also be performed on gray-scale or color images.

Thresholding. The simplest method for segmenting an image is to use thresholding techniques. Thresholding may be performed on monochrome or color images. For monochrome images, pixels within a particular gray-scale range or value may be displayed on a computer monitor and the analysis performed on the displayed pixels. Greater discrimination may be achieved using color images. Image segmentation may be achieved based upon red, green, and blue (RGB) values in the image; a more powerful method is to use hue, saturation, and intensity (HSI). The HSI method of color discrimination is closer to that of the human brain. Depending upon the image, it may be possible to achieve discrete identification of objects based on threshold alone. However, for gray-scale electron microscopic images, thresholding may only work for simple specimens (i.e., count negatively stained virus particles). It is seldom sufficient to identify the objects of interest in complex specimens (sections of a cell or tissue) because many disparate objects often share similar gray-scale levels.

Another method to segment the image is edge detection. Edge-detection filters such as Laplace, Sobel, and Roberts will detect and enhance individual objects. However, these filters may still leave some objects with discontinuous boundaries and will fail to separate objects that touch each other. Algorithms may be used to connect nearby edges, and watershed filters may be used to separate touching objects. When images are segmented it is then useful to use additional parameters to classify the objects. One useful parameter is shape. The *shape factor* of an object is defined as $4\pi \times (\text{area})/(\text{perimeter})^2$. A perfect circle will have a shape factor of 1. Departure from circularity (e.g., oval or irregular border) will lower the shape factor. The shape factor can also be expressed as $(\text{perimeter})^2/(\text{area})$. With this formula, a circle has a minimum value of 4π and the factor becomes larger for noncircular objects. This is a useful criterion for distinguishing cancer cells from normal cells. Cancer cells or their cell nuclei usually are less circular than normal cells. In addition to shape, size features such as minimum and maximum diameter or area may be included.

Enumeration. One of the simplest procedures in image analysis is the *counting of objects.* If a digital image is displayed in any of a variety of image analysis software programs, one has the option of identifying a *region of interest* (ROI) for analysis. In most circumstances it is important that the area chosen for analysis be derived via systematic sampling, and not because the area has the features of interest. The entire image may be the ROI, or a polygonal or irregular region may be specified. The bounding box of the image in Fig. 13 is the ROI.

If a threshold is set using a software program for image analysis, the features will be identified via the RGB or gray-scale color values and a boundary identified for the objects. The objects are then counted, omitting any that touch the ROI, since these may be partial profiles. In the preceding example the number of profiles is 26.

Up to this point, the discussions of image analysis are those applied to model-based systems. In model-based systems, algorithms are used to extract the quantitative data. However, these morphological operations make certain assumptions about the nature of the objects being measured, and therefore have some inherent bias in the measurement process. Image analysis based upon modern stereological methods utilizes probabilistic geometry to extract quantitative information from images. Because the data are extracted via systematic sampling and point counting, no assumptions are made as to the size or shape of the structures and the technique may therefore be considered an unbiased method of analysis.

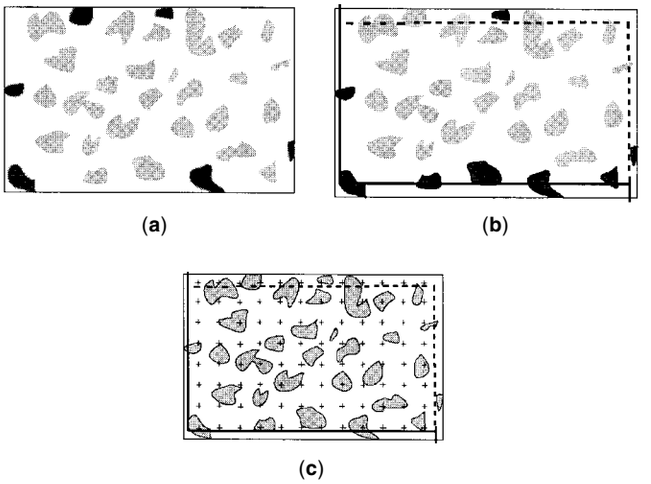

Figure 13. Bounding boxes depict ROI.

Using the methods of modern stereology, an unbiased counting frame is placed over the image used for counting objects. Every profile completely within the counting frame is tallied along with those that touch the upper and right dashed line. Profiles touching the solid line are excluded from the tally. The result is 24 profiles counted [Fig. 13(b)].

If the size of the counting frame is known, the number of profiles may be expressed as numerical density (the number of objects divided by the frame area). If we assume arbitrarily that the frame represents 10 μm^2, then the numerical density (Q_A) = 24/10 μm^2 = 2.4 objects per μm^2. After counting the number of objects, the next basic operation is to determine the size or area of the objects.

If a counting frame with regularly spaced points is placed over Fig. 13(c), then the mean areal fraction of the objects may be determined. A profile is counted if it covers the upper right quadrant of one of the counting points on the grid. The points are counted with no regard to their relationship to the counting frame. The areal fraction A_A is defined as the number of points hitting profiles divided by the total number of points

$$A_A = 16/96 = 0.166$$

This value may be used to determine the mean profile area provided the area of the frame is known. The mean profile area $a = A_A/Q_A$, where Q_A is the relative number of profiles.

$$Q_A = 24/10\,\mu m^2 = 2.4/\mu m^2$$

Therefore the mean area a = 0.166/2.4 = 0.069 μm^2.

Volume Estimation. These same principles of image analysis utilized to extract information from 2-D images may be extended and modified to extract data from 3-D images. In model-based image analysis, algorithms would be used to estimate volumes of structures. The volumes of structures may be determined from serial sections of material obtained through a confocal microscope (optical sections) or plastic (epoxy) -embedded sections of tissues. If the thickness of a section is known, the volume may be determined by summing the areas of the segmented objects of interest. Some software programs are able to do a seed fill of such structures so that the entire object is visualized and then algorithms used to estimate volume. Instead of seed filling, a wire frame may be placed around an object and an isocontoured surface applied to the image. Algorithms may then be used to estimate the surface area of the 3-D object. Using design-based stereology, 3-D information may be extracted from 2-D sections of objects as shown in Fig. 14(a).

The Cavalieri method can be used to estimate the volume of compartments within a structure (i.e., an organ such as the lung or liver). From a random starting point, the structure is sliced systematically. The random start point is determined by dividing the length of the structure by some slice interval: a 100 mm structure divided by 10 gives a slice interval of 10 mm. To determine the position of the first slice, a random number between 1 and 10 is chosen (e.g., 4 mm).

After processing and embedding the slices, the area of the slices may be determined by point counting methods. The volume of the structure $V(\text{struct}) = \Sigma P(\text{struct})\ A(\text{point})nt$, where $\Sigma P(\text{struct})$ is the sum of all points falling on the slices, $A(\text{point})$ is the area of a test point at a magnification of one, n is the nth slice selected, and t is the mean thickness of the slice.

The analysis in three dimensions may also be used to estimate the numerical density of objects (i.e., cells) within a structure (tissue or organ) using an optical dissector. The dissector is a direct counting method. Plastic sections (~40 μm to 50 μm) are examined under the light microscope, and as one slowly focuses down through the section, each cell nucleus that appears is counted. The vertical movement of the stage is the height of the dissector. In Fig. 14(b), each numbered section represents an optical section. The volume of the tissue

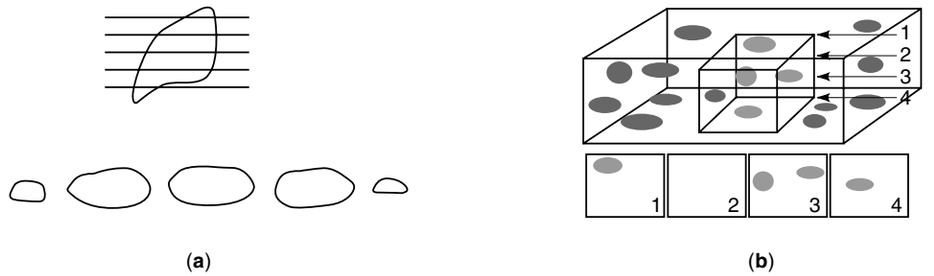

Figure 14. (a) 3-D information extracted from 2-D sections of objects; (b) numbered sections represent an optical section.

containing the cells is determined by the area of the dissector counting frame (i.e., 0.5 mm^2) multiplied by the dissector height. The number of cells divided by the dissector volume equals the 3-D numerical density of the cells. The numerical density multiplied by the volume of a structure V(struct) would then equal the total number of cells in the structure.

Data Storage for Image Analysis

Storage mediums are also undergoing rapid development. Storage onto computer hard-disk drives should be considered only temporary until the images are archived. The most cost-effective and platform-portable storage method is archiving images onto recordable read-only memory compact disks (CD-ROMs). Since almost all personal computers now have CD-ROM drives, this archival method provides accessibility for most users without the need for specialized equipment. Storage of images in ISO-9660 format guarantees readability of the images on Microsoft Windows, UNIX, and Apple computers. CD-ROMs have an expected shelf life of 30 to 100 years depending upon how they are used and stored. The successor to the CD-ROM is the digital versatile disk (DVD). Currently, DVD players cannot read CD-ROM, because the wavelength of the DVD laser is different from what is required for CD-ROM. It is possible that manufacturers will provide DVD readers with dual lasers so that there will be some backwards compatibility, but eventually data stored on CD-ROM may have to be transferred to other media. Of the tape storage solutions, digital linear tape (DLT) has the quickest access times and may be a possible solution for mass storage.

MEDICAL APPLICATIONS

Laser Scanning Ophthalmoscopy

Recently a near-infrared laser scanning ophthalmoscope was developed that could look deep into the macula region, the central region of the retina where the high density of rods and cones results in the eye's high resolution. This instrument uses a vertical-cavity surface-emitting laser (VCSEL) array laser operating at 850 nm. The instrument combines a regular ophthalmoscope and a laser confocal ophthalmoscope. The advantage of the near-infrared light is that it passes through the somewhat opaque lens common in patients with cataracts.

HARDWARE

Microscopes

Many companies manufacture microscopes and all make relatively high-quality instruments. Some of the better known are Leica, Olympus, Nikon, and Zeiss. All these companies currently manufacture confocal microscopes as well. Bio-Rad Microsciences, Meridian Instruments, Molecular Dynamics, Noran, Newport, and Optiscan all manufacture confocal microscopes based upon the above commercially available microscope systems.

BIBLIOGRAPHY

R. P. Bolender, Biological stereology: History, present state, future directions, *Microsc. Res. Tech.* **21**: 255–261, 1992.

R. P. Bolender, D. M. Hyde, and R. T. Dehoff, Lung morphometry: A new generation of tools and experiments for organ, tissue, cell, and molecular biology, *Amer. Physiol. Lung Cell. Mol. Physiol.* **265**: L521–L548, 1993.

L. M. Cruz-Orive, Particle number can be estimated using a disector of unknown thickness: the selector, *J. Microsc.* **145**: 121–142, 1987.

H. J. G. Gundersen and E. B. Jensen, The efficiency of systematic sampling in stereology and its prediction, *J. Microsc.* **147**: 229–263, 1987.

H. J. G. Gundersen et al., Some new, simple and efficient stereological methods and their use in pathological research and diagnosis, *Acta Pathol. Microbiol. Immunol. Scand.* **96**: 379–394, 1988.

B. Matsumato (ed.), *Cell Biological Applications of Confocal Microscopy,* Vol. 38 of Methods in Cell Biology, San Diego: Academic Press, 1993.

J. B. Pawley (ed.), *Handbook of Biological Confocal Microscopy,* 2nd ed., New York: Plenum, 1995.

J. C. Russ (ed.), *The Image Analysis Handbook,* 2nd ed., Boca Raton: CRC Press, 1995.

J. Serra, *Image Analysis and Mathematical Morphology,* London: Academic Press, 1983.

D. L. Spector, R. D. Goldman, and L. A. Leinwand, *Cells: A Laboratory Manual,* Vol. 2, Light Microscopy and Cell Structure, New York: Cold Spring Harbor Laboratory Press, 1998.

Y.-L. Wang and D. L. Taylor, *Fluorescence Microscopy of Living Cells in Culture,* San Diego: Academic Press, 1989.

J. PAUL ROBINSON
JOHN TUREK
Purdue University

MICROSCOPY, ACOUSTIC. See ACOUSTIC MICROSCOPY.
MICROSCOPY, MAGNETIC. See MAGNETIC MEDIA, IMAGING.
MICROSCOPY, X-RAY. See X-RAY MICROSCOPY.
MICROSENSORS. See PIEZORESISTIVE DEVICES.
MICROSOFT WINDOWS. See WINDOWS SYSTEMS.
MICROSTRIPLINE. See STRIPLINE COMPONENTS.